



Universiteit  
Leiden  
The Netherlands

## Towards superconducting spintronics with RuO<sub>2</sub> and CrO<sub>2</sub> nanowires

Prateek, K.

### Citation

Prateek, K. (2023, December 8). *Towards superconducting spintronics with RuO<sub>2</sub> and CrO<sub>2</sub> nanowires*. *Casimir PhD Series*. Retrieved from <https://hdl.handle.net/1887/3666050>

Version: Publisher's Version

License: [Licence agreement concerning inclusion of doctoral thesis in the Institutional Repository of the University of Leiden](#)

Downloaded from: <https://hdl.handle.net/1887/3666050>

**Note:** To cite this publication please use the final published version (if applicable).

# 4

## Moving Domain Walls in Permalloy and CrO<sub>2</sub> Nanowires

*The manipulation of domain walls (DW) in ferromagnets using current or pulse-driven techniques has been the subject of research for almost two decades, and its fundamental tenets have been extensively explored. One significant limitation is the relatively high threshold current ( $J_c$ ) of  $10^{12}$  A/m<sup>2</sup> for moving DW in traditional ferromagnets which are not fully spin-polarized, resulting in substantial Joule heating. In contrast, half-metallic ferromagnets like CrO<sub>2</sub> holds the promise to lower  $J_c$ . In this work, we built a high frequency setup to allow injection of current pulses and investigated the pinning and depinning of DW using a triangular constriction (notch) in two ferromagnets: Permalloy, as a reference material and CrO<sub>2</sub> to study a fully spin-polarized material. We have also characterized domain wall resistance in CrO<sub>2</sub>, and found it to decrease from 25 m $\Omega$  at 10 K to 18.2 m $\Omega$  at 80 K, then rise to roughly 23 m $\Omega$  at 300 K. We find that in general, the notch size affects  $J_c$ . While a deep notch (> 50% of wire width) increases the DW resistance, it also leads to strong pinning potential for both Py and CrO<sub>2</sub> samples which makes depinning difficult. Additionally, CrO<sub>2</sub> devices are more sensitive to the notch depth, with a 5% deeper notch on a wire of similar size results in a 2.5 times higher  $J_c$ . The depinning critical current densities in CrO<sub>2</sub> are comparable to that of Py samples and are unaffected by strong spin polarization.*

## 4.1. Introduction

Over the past two decades, spintronics has been at the forefront of research in the pursuit for CMOS alternatives for next-generation 3D data storage and logic devices [1]. One such approach is a “racetrack” memory that uses magnetic domains to store information [2]. Architectures relying on magnetic domain walls leverage the benefits of high velocity, high density, non-volatility and flexible design of domain walls to process and store information. These systems rely on controlled movement between precise distinct positions of domain walls in magnetic elements, such as a ferromagnetic wire, where a domain wall (DW) is formed at the boundaries between magnetic domains magnetized in opposite directions. Patterned geometrical traps, artificial constrictions, or others, are utilized to precisely locate DW and produce an attractive pinning potential. Traditionally magnetic fields were employed to manipulate DWs. A magnetic field however, cannot facilitate the simultaneous movement of many domain walls in the same direction, making it unsuitable for DW-motion-based memory systems. Since the pioneering work of Berger *et al.* on current-driven domain-wall motion [3], the spin-transfer torque has been recognized to be useful in manipulating magnetization in nanomagnets.

Most of the studies on current-induced DW motion have been done on conventional ferromagnets like permalloy (Py) or Co. A threshold current  $J_c$  on the order of  $10^{12}$  A/m<sup>2</sup> was observed for DW-motion in Py nanowires [4] and Py rings [5]. Kläui *et al.* also showed that pulse injections can transform domain structure from a vortex wall to a transverse wall. Others have also made similar observations [6]. An important drawback of these studies is the high  $J_c$  which leads to increased nanowire temperature due to Joule heating [7]. In severe instances, nanowire temperatures can even reach the Curie temperature  $T_C$ . In comparison, CrO<sub>2</sub>, a half-metal ferromagnet with 100% spin polarization holds the promise to lower  $J_c$  [8]. There have been several attempts with limited success to investigate the pinning and depinning of DW in CrO<sub>2</sub> [9, 10]. Biehler *et al.* fabricated CrO<sub>2</sub> wire of widths (0.5-2)  $\mu\text{m}$  from full films using Ar-etching and found that a pulse of duration 10  $\mu\text{s}$  corresponding to a  $J_c$  of  $5 \times 10^{10}$  A/m<sup>2</sup> was required to alter the magnetic domain configurations at room temperature. However, the pulses led to increase in the sample temperatures beyond  $T_C$ . More recently, Chen *et al.* investigated the DW resistance in an anvil-shaped epitaxial CrO<sub>2</sub> structure. Their structure allowed the generation and annihilation of a DW by measuring the resistance jump between a single-domain state and a domain-wall state through field sweeps [11]. However, a precise control and manipulation of DW through currents on CrO<sub>2</sub> has not yet been performed.

Experiments on moving domain walls (DWs) can take different forms. One way is to induce a DW in a wire  $F_1$  by sending a current pulse through a cross-wire,

inducing the DW in  $F_1$  by the Oersted fields of the current. By also applying a current in  $F_1$ , the DW can then be moved [12, 13]. Here, we address a slightly different question. Using a ferromagnetic wire with a narrow triangular constriction (a so-called 'notch'), we first pin a DW in the constriction by applying small in-plane magnetic fields. We detect the presence of the DW by measuring the anisotropic magnetoresistance (AMR) of the wire and observing a change in resistance when the DW is caught. Then we use pulsed currents to find the critical current  $I_c$  that depins the DW again. A magnetic field can be applied to investigate its effects on  $I_c$ . In this work, we investigate the pinning and depinning of domain walls on Py and  $\text{CrO}_2$  nanowires and compare the results.

## 4.2. Experimental setup

The MR measurements were performed in a Physical Property Measurement System (PPMS) that could be cooled down to a base temperature of 2 K. We used a Keithley model 6221 low Noise Precision AC/DC Current Source to provide dc currents and a Keithley model 2182A digital nanovoltmeter to measure voltage. Firstly, two-probe measurements were performed at room temperature to characterize a new sample and confirm that all contact leads and connected nanostructures were intact. Next, we connected the sample in a four-point method as shown in Fig. 4.1(a), with the inner leads for the voltage and the outer leads for the current, allowing a direct measurement of sample resistance without the contact wire resistance. Samples were routinely cooled down to 10 K for the measurements. For the pulsed current measurements, we designed and developed a high-frequency pulse generator in-house. The schematics for this will be presented later.

We used two different ferromagnets for the experiments. Permalloy (Py) was used as a reference material, because much is known about DW motion in this weakly anisotropic material with medium-sized spin-polarization.  $\text{CrO}_2$  was used to study the situation of a fully spin-polarized material, for which actually only few experiments exist. We used similar dimensions for the Py and  $\text{CrO}_2$  wires. Below, we first discuss the sample fabrication, the characterization of the notched wires by magnetotransport measurements, and we present the setup for generating current pulses. The latter comes in two flavors. With the initial design that reached current densities around  $2 \times 10^{11}$  [A/m<sup>2</sup>], DWs could be depinned in the Py wire, but not in the  $\text{CrO}_2$  wire. The modified design increased the applied current by an order of magnitude, and allowed depinning to be observed in both wires.

### 4.2.1. Sample fabrication

CrO<sub>2</sub> devices were grown using the Selective Area growth technique via Chemical Vapor Deposition as described in detail in sec. 3.2. We also fabricated Permalloy (Py) nanowires with Cu contacts for pulse measurements as a standard device to test our experimental setup. To make Py devices, we first patterned the desired nanostructures on a Si substrate that has a 300 nm wet thermal oxide layer on top, using electron beam lithography. The Py was then deposited using e-beam evaporation at a very low pressure of  $8 \times 10^{-9}$  mbar, which was followed by a lift-off process to obtain the central Py structure as shown in Fig. 4.3 (in gray). Subsequently, to make Cu contacts on the Py nanowire, we patterned the contacts using e-beam lithography. This was followed by Ar etching to remove the top dead layer of Py before e-beam evaporation of Cu and lift-off steps. For both the CrO<sub>2</sub> and Py devices, the notch was made in the center of the nanowire using Focused Ion Beam (FIB) milling. In our samples, we used two types of notch : single notches (a triangular shape pointing inward from one side of the wire) or double notches (two triangles pointing inward from the two sides). They act as artificial pinning centers for the domain walls.

### 4.2.2. Sample characterization

**CrO<sub>2</sub> devices:** We designed a CrO<sub>2</sub> device as shown in Fig. 4.1(a) consisting of a central CrO<sub>2</sub> wire of width = 500 nm, and length between the inner contact leads ( $V^+$  and  $V^-$ ) = 1.5  $\mu\text{m}$ . The centre of the wire has a double notch where the width of the CrO<sub>2</sub> wire had been reduced to 91 nm. The left end the CrO<sub>2</sub> wire consists of a large contact pad. It ensures that the central CrO<sub>2</sub> wire has a different switching field than the contact pad. This is necessary for the nucleation of the domain wall in the contact pad, which then propagates along the wire through the notch (if not pinned) and terminates at the right end of the wire, which has a pointed shape. The movement of the domain wall is always from the contact pad to the wire, regardless of the direction of the magnetic field, as it is energetically favorable. Conversely, it is energetically prohibited for the domain wall to travel from the wire to the contact pad, preventing its movement from the right end of the wire to the left.

The growth of the CrO<sub>2</sub> nanowire was immediately followed by electrical characterization. We measured the resistance  $R$  as a function of the temperature  $T$  of the nanowire before and after FIB milling. As seen in Fig. 4.1 (b) (green curve), the resistance at room temperature (300 K) is 96.2  $\Omega$  which corresponds to a resistivity  $\rho_{300}$  of 190  $\mu\Omega\cdot\text{cm}$  while the resistance at low temperature (10 K) is 6.9  $\Omega$ , corresponding to  $\rho_{10}$  of  $\sim 12 \mu\Omega\cdot\text{cm}$ . This gives a residual-resistivity ratio (RRR, the ratio between  $\rho_{300}$  and  $\rho_{10}$ ) of about 16. Next, using FIB, we made a double notch and

## 4.2. Experimental setup

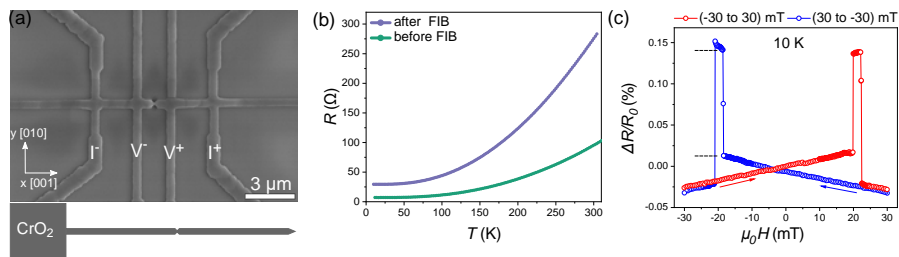


Figure 4.1: (a) SEM image of a  $\text{CrO}_2$  device used in this study (see details in the text). The wire axis is along the  $[001]$  direction. The four contact leads ( $I^+$ ,  $I^-$ ,  $V^+$  and  $V^-$ ) are used for the four-point resistance measurement. The contacts leads are also made of  $\text{CrO}_2$ . The center of the wire contains a narrow constriction of the double notch type made with using Focused Ion Beam milling. The bottom part of the image shows the full design of the  $\text{CrO}_2$  wire where the contact pad is at the left end of the wire and the right end has a pointed edge termination. (b) Resistance of the  $\text{CrO}_2$  device as a function of temperature from 300 K down to 10 K before making the notch (green) and after the notch (purple). (c) In-plane longitudinal magneto-resistance along  $[001]$  as measured at 10 K by sweeping the magnetic field from  $-30$  mT to  $+30$  mT and back.  $R_0$  was measured to be  $28.34 \Omega$ . The step size is  $0.5$  mT. The interval between the dotted lines in (c) defines  $\Delta R_{DW}$ . The current used in both resistance and MR measurement is  $100 \mu\text{A}$ .

measured  $R(T)$  again (Fig. 4.1(b) purple curve). We notice a rise in the resistance both at room temperature and at 10 K. The RRR value is now  $\sim 9$ . We estimated the resistance of the notched part of the wire. Assuming that the  $\rho_{10}$  stayed the same, we get a resistance  $R_{notch}$  of  $3.84 \Omega$ . But, the total resistance of the wire after FIB is around  $29 \Omega$  which suggests either some FIB damage, which would increase resistivity, or a decrease of thickness (the same). The observed reduction in RRR, a measure of crystal quality can then be attributed to the damage from the Ga ions to  $\text{CrO}_2$  nanowire during FIB process.

We further performed magnetoresistance (MR) measurements at 10 K. Fig. 4.1(c) shows the longitudinal MR behavior defined as  $[R(\mu_0 H) - R_0]/R_0 = \Delta(R)/R_0$ , where  $\mu_0 H$  is the magnetic field along the wire axis  $[001]$  which is also the magnetic easy-axis of  $\text{CrO}_2$  and  $R(0) \equiv R_0$  is the resistance at zero field. The value of  $R_0$  in Fig. 4.1(c) is  $28.34 \Omega$ . Initially, the field was kept at  $-500$  mT so that the magnetization direction of both the wire and the contact pad was along the negative x-axis. We then reduced the field to  $-30$  mT before starting the measurement. We swept the field in steps of  $0.5$  mT until  $10$  mT. After that the step size was decreased to  $0.1$  mT from  $10$  mT until  $25$  mT. Thereafter, the step size was increased to  $0.5$  mT until we reached  $30$  mT. This completes the first half of the measurement (blue curve in Fig. 4.1(c)). The field was then increased to  $+500$  mT to saturate the magnetization direction of both the wire and contact pad, but now along x-axis, and the same steps of field sweep were done, now from  $+30$  mT until  $-30$  mT (red curve in fig. 4.1(c)) to finish the loop.

The MR loop shows a high resistance state between 19.9 mT and 22.1 mT and between  $-18.5$  mT and  $-20.9$  mT. This can be understood by contemplating the magnetic domain state. The magnetic easy axis of CrO<sub>2</sub> is along [001], which is parallel to the wire axis of our device. As mentioned above, the difference in the size of the wire and contact pad ensures different switching fields for them. In this case the contact pad will switch magnetization at lower fields because it has a larger area. At  $\pm 500$  mT, both the central wire and the contact pad have a uniformly aligned parallel magnetization along the  $\pm x$  axis respectively. At  $-30$  mT, the magnetization is still homogeneous, and the resistance measured between  $V^+$  and  $V^-$  is low. Next, we gradually increase the field to 30 mT. The magnetization of the contact pad starts to switch, and at 19.9 mT, the wire starts to switch, meaning a DW propagates along the length of the wire. The field helps in the movement of the DW and it gets pinned at the notch, leading to the higher resistance  $R_{high}$ . The DW remains pinned with further increase of the field until 22.1 mT. Beyond that, the DW depins and moves out of the wire at the pointed end. The resistance returns to its lower value  $R_{low}$  between 22.2 mT and 30 mT. Similarly, when we sweep the field from  $+30$  mT to  $-30$  mT, we obtain a high resistance state between  $-18.5$  mT and  $-20.9$  mT. The slight asymmetry in the (de)pinning fields is due to the asymmetry in the device coming from the edges of the wire and the notch.

Next, we performed MR measurements at different temperatures and calculated the evolution of  $\Delta r_{DW} = R_{high} - R_{low}$  for each temperature. Fig. 4.2 (a) and (b) show MR measurements done at 50 K and 100 K as an example. Fig. 4.2(c) gives the plot of  $\Delta r_{DW}$  as a function of temperature from 10 K to 300 K. We find a weak temperature dependence over the entire temperature range.  $\Delta r_{DW}$  decreases slightly from  $25.7 \pm 1.5$  m $\Omega$  at 10 K to  $18.2 \pm 1.1$  m $\Omega$  at 80 K. Above 80 K,  $\Delta r_{DW}$  appears to increase again reaching a value of around 23 m $\Omega$  at 300 K. Fig. 4.2 (d) shows temperature dependence of ratio  $\Delta r_{DW}/R_0$ . We found that as temperature increased  $\Delta r_{DW}/R_0$  decreased monotonically.

We calculate the area of the DW of CrO<sub>2</sub> wire (see 4.1 (a)) from the depth of notch (d) of 91 nm and wire thickness (t) of 60 nm. Then, the resistance-area product for the DW is defined as  $RA_{DW} = \Delta r_{DW} \times d \times t$ . At 10 K, we obtain  $RA_{DW}$  of  $1.4 \times 10^{-16}$   $\Omega\text{m}^2$ , which is comparable to the values reported for LSMO nanostructures [14] and other conventional ferromagnets like Co and Py [15]. However, this value is around 3 orders of magnitude smaller than  $RA_{DW}$  of  $0.65 \times 10^{-13}$   $\Omega\text{m}^2$  at 77 K reported by ref. [16].

It is instructive to compare  $\Delta r_{DW}$  and  $\Delta r_{DW}/R_0$  data with experiments reported by Chen *et al.*[11], who performed measurements on a slightly different geometry. Rather than a notch in the middle of a wire, they used a CVD-grown structure with the shape of a sharp point into anvil. A DW can be caught at that point contact

## 4.2. Experimental setup

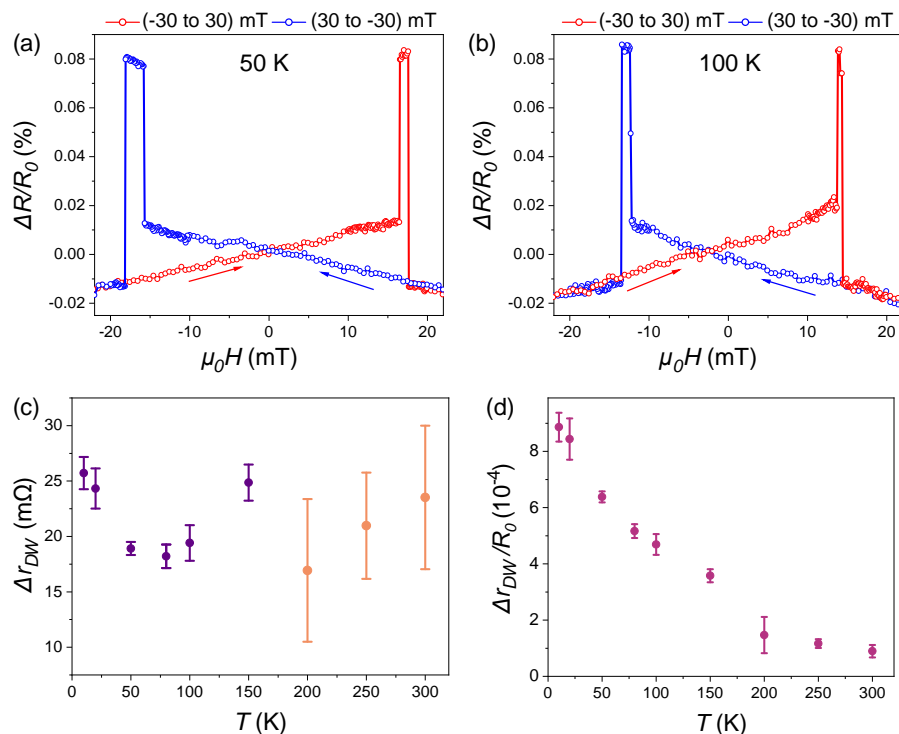


Figure 4.2: Two MR measurements on the same CrO<sub>2</sub> device as used in Fig. 4.1, with the magnetic field along [001] at (a) 50 K, where  $R_0 = 29.64 \Omega$  and (b) 100 K, where  $R_0 = 41.32 \Omega$ . The field was swept between 25 mT and -25 mT. The step size is 0.5 mT. The current used for both is 100  $\mu$ A. (c) Resistance difference ( $\Delta r_{DW}$ ) between the high-resistance and the low-resistance states as a function of temperature, showing a weak temperature dependence over the range from 10 K to 300 K. (d) Temperature dependence of ratio  $\Delta r_{DW}/R_0$  indicates that as temperature increases  $\Delta r_{DW}/R_0$  decreases. Multiple measurements were done for each temperature to calculate the error bars indicating the data fluctuations.

(where the width of the constriction is 50 nm), and they could measure  $\Delta r_{DW}$  and  $\Delta r_{DW}/R_0$  (in our terminology). Their values for the DW resistance (DWR) are significantly smaller (around 4.5 mΩ), indicating a different wall structure, but they also find a decrease with increasing temperature until about 80 K. Then  $\Delta r_{DW}$  rises sharply and reaches values an order of magnitude higher than the value at low temperature. They argued that there are two competing temperature-dependent terms in play, spin-dependent scattering and spin disorder, both to be assessed in the DW. Following Levy and Zhang [17], and Viret [18],  $\Delta r_{DW}/R_0$  for currents perpendicular to the wall depends on a factor  $(\alpha - 1)^2/\alpha$ , with  $\alpha = \rho_0^\uparrow/\rho_0^\downarrow$ , where  $\rho_0^{\uparrow,\downarrow}$  are the spin-dependent resistances. When the minority spin channel is populated by e.g. spin excitations (magnons),  $\alpha$ , and therefore the DWR, will decrease with increasing temperature. Furthermore, it stands to reason that spin disorder will

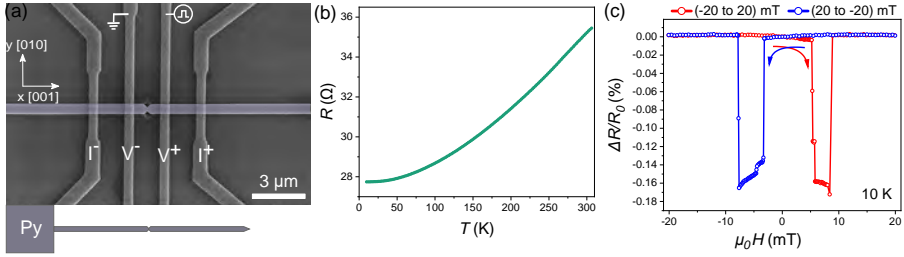


Figure 4.3: (a) SEM image of a Py device (Py wire shown in false color is along [001]) used in this study (see details in the text). The contacts leads are made of Cu. The four contact leads ( $I^+$ ,  $I^-$ ,  $V^+$  and  $V^-$ ) are used for the four-point resistance measurement. The center of the wire has a narrow constriction (a double notch) made by Focused Ion Beam milling. The bottom part of the image shows the full design of the Py wire where the contact pad is at the left end of the wire while the right end has a pointed edge termination. (b) Resistivity of the Py device as a function of temperature from 300K down to 10 K after the notch. (c) In-plane longitudinal magneto-resistance along [001], measured at 10 K by sweeping the magnetic field between 20 mT and  $-20$  mT. The step size is 0.5 mT. The current used in both resistivity and MR measurements is 100  $\mu$ A.

increase with increasing temperature. That the spin disorder wins from the spin-dependent scattering above 80 K may be connected to the appearance of skyrmion-like topological defects in the magnetic state of CrO<sub>2</sub> [19, 20] that not only effect the bulk, but also the DW.

**Py-Cu devices:** We also made Py nanowires with Cu contacts using the fabrication steps described in detail in sec. 4.2.1. The Py nanowire (along [001]), as shown in fig. 4.3(a) has the following dimensions: width ( $w$ ) = 500 nm, thickness ( $t$ ) = 50 nm and the length ( $l$ ) = 1.5  $\mu$ m (between  $V^+$  and  $V^-$ ). The centre of the wire has a double notch where the width of the Py wire is 165 nm. We characterized the device by first measuring resistance as a function of temperature. As shown in Fig. 4.3(b),  $R(300\text{ K})$  is 35.23  $\Omega$  while  $R(10\text{ K})$  is 27.74  $\Omega$ . This gives a typical residual-resistivity ratio of 1.3 which is quite low compared to CrO<sub>2</sub>. Since Py is a disordered alloy, this is to be expected.

We next measured the MR hysteresis loop by sweeping field along the  $\pm x$ -axis of the wire between  $\pm 20$  mT. We followed the same protocol as for CrO<sub>2</sub> sample. As shown in Fig. 4.3(c), the resistance of the homogeneously magnetized state is now higher than the state in which a domain wall is trapped by the notches. Again this is a well known effect, caused by the fact that for these  $^3d$  magnets, the resistance is lower when the current is perpendicular to the magnetization, which is the situation for the domain wall in the notch. We obtain the low resistance state in between 5.2 mT and 8.9 mT and from  $-7.9$  mT to  $-3.3$  mT.

## 4.2. Experimental setup

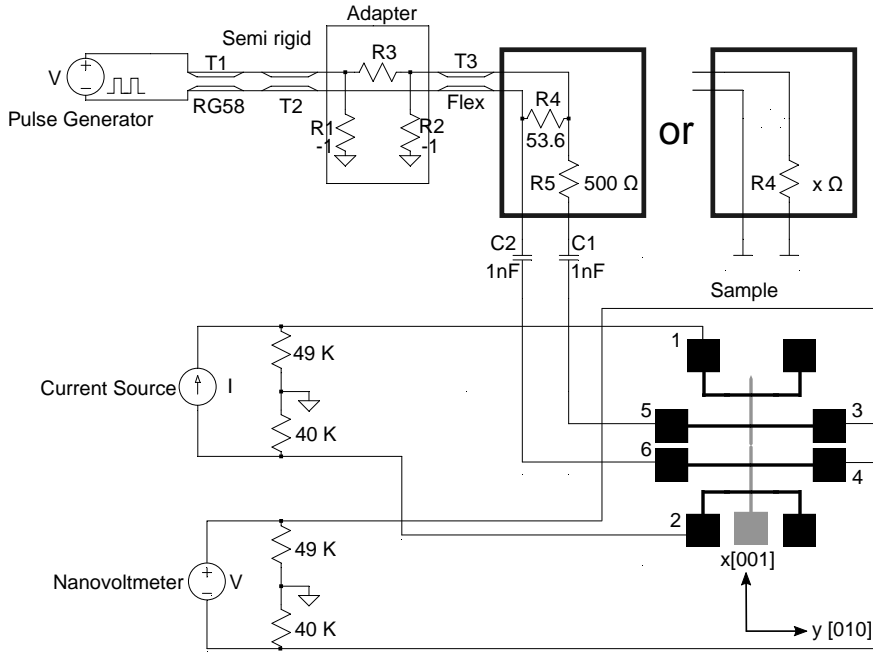


Figure 4.4: Schematic diagram illustrating the circuit design employed in the high frequency setup used for pulse injection. See detailed description in the text. The two rectangular boxes separated by "or" in between show the two different ways the current limiting resistances were designed. The left box depicts the configuration for the initial setup. The revised version, shown in the right box, incorporates a variable resistance (shown as " $x\Omega$ ") instead of  $R_4$  and  $R_5$ , enables the injection of current by an order of magnitude larger as compared to the initial setup. In the circuit diagram following notations have been used. V: Voltmeter, RG: Radio Guide, R: Resistance, C: Capacitance. Crystal Orientation of the sample is also displayed. The easy axis of the  $\text{Py}/\text{CrO}_2$  device shown in grey lies along  $[001]$  direction.

### 4.2.3. High frequency setup for pulse injection

We designed and developed a high frequency setup in-house that could be used to inject pulses to study current-induced domain wall motion. For this, the general purpose PPMS multi-functional probe insert (model 450A) was modified. Apart from the mechanical modifications made to accommodate the parts needed for sample holding, thermal anchoring etc., two semi rigid co-axial cables were introduced in the insert, which were connected to a pulse generator at one end and to the sample at the other end as shown in Fig. 4.4. The circuit was designed to achieve impedance matching as close as possible to  $50\Omega$ . This design objective aims to minimize loss and maximize power and voltage of the pulse that is fed to the sample. We used an Instek AFG-3081 80 MHz Arbitrary Function Generator for pulse injection. The internal output resistance of  $50\Omega$  of the pulse generator

was connected to contacts 5-6 of the sample, schematically shown in the Figure. For our measurements, we applied square pulses of the following parameters : frequency = 10 MHz, duty cycle = 20% while amplitude is varied. The two rectangular boxes separated by “or” in between show the two different ways the current limiting resistances were connected. The left box depicts the configuration for the initial setup. The revised design, shown in the right box, incorporates a variable resistance (shown as “x”  $\Omega$ ) instead of R4 and R5, hence allowing the injection of a current into the devices we used, that is an order of magnitude larger compared to the initial setup.

In order to determine the combinations of current and field that result in domain wall motion, the following experimental sequence was executed multiple times for each combination of field strength, current density of the pulse, and temperature:

- (i) A full MR hysteresis loop was measured to get an idea about the switching fields for different states i.e. the single domain state or a DW pinned at the notch (as an example shown in Fig. 4.1(c)).
- (ii) Then, a field driven DW motion experiment was performed to observe the critical pinning and depinning fields without injecting pulses (as an example shown in fig. 4.5)
- (iii) Next, the pulse measurements were done similar to the last step: the DW is first pinned with the help of the field. Then the field was changed to a desired value where we wanted to depin the DW. Then square pulses of the desired amplitude, time-period and the pulse count were injected (as an example shown in fig. 4.6).
- (iv) The resistance values were continuously measured, and if the resistance changed and returned to the value of the single domain state, it would be interpreted as the depinning of the DW from the notch. The experiment was repeated multiple times to check its reproducibility (as an example shown in fig. 4.7(b)).
- (v) The field was changed and step (iii) and (iv) were repeated in order to determine the dependence of the (de)pinning critical current on an applied magnetic field ('field-assisted depinning').

Pulses were applied as voltage pulses. For the initial high frequency set up the current can be extracted as  $I = V / (500 + R_s)$  where  $V$  is the amplitude of pulse and  $R_s$  is the device resistance. For the revised set up  $I = V / (x + R_s)$  where “x” is the variable resistance added in series with device to make the total resistance as close

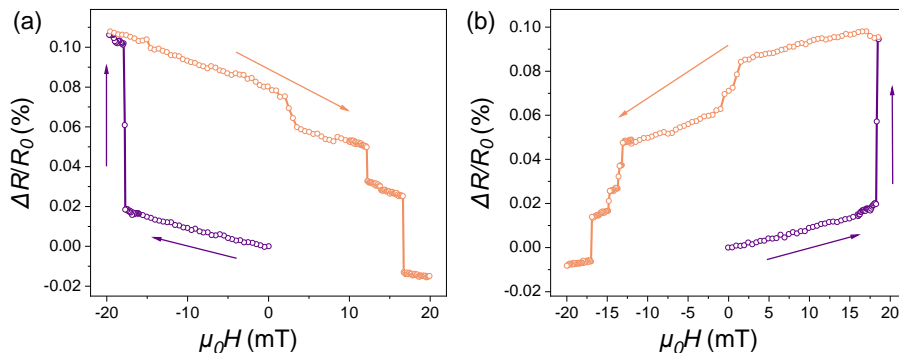


Figure 4.5: Field-driven DW motion. (a) The field is swept from 0 mT to  $-19.5$  mT (the pinning field) where  $R$  jumps to the high resistance state (purple curve). Next, the field is swept back until the low resistance state (orange curve) is reached at  $16.7$  mT (the depinning field). (b) Same as in (a) but in the reversed direction. We find the pinning field at  $18.5$  mT and the depinning field at  $-17$  mT.

as possible to  $50 \Omega$ . Using the size of the device, the critical depinning current density can be computed. Estimating the size of these voltage pulses at the position of the sample is difficult because of reflection and losses in the leads, so we made an estimate with a table-top experiment, which led to the conclusion that it is of the order of 22% of the amplitude of the applied voltage. We have taken this factor into account when computing the current density.

### 4.3. Investigating domain wall motion in CrO<sub>2</sub> nanowires

We used the same CrO<sub>2</sub> sample as shown in Fig. 4.1 (a) of  $w = 500$  nm,  $t = 60$  nm and  $l = 1.5 \mu\text{m}$ . The centre of the wire has a double notch where the width of the CrO<sub>2</sub> wire is  $91$  nm. The sample was connected to the high frequency setup which was initially designed in the left rectangular box configuration as shown in Fig. 4.4. We applied a constant d.c. current of  $100 \mu\text{A}$  between contacts 1 and 2 and measured the voltage between the contact 3 and 4. The field was applied along the central CrO<sub>2</sub> nanowire axis (shown in grey in Fig. 4.4) which was along  $\pm x$ , which is also the easy magnetic axis of CrO<sub>2</sub>. The temperature was set to  $10$  K.

#### 4.3.1. Field-driven measurements on CrO<sub>2</sub>

We measured the full MR hysteresis loop as shown in Fig. 4.1(b) during the characterization of the sample. Next, we investigated field driven DW motion as shown in Fig. 4.5(a,b). In Fig. 4.5(a), the field was first set to  $+500$  mT to saturate the magnetization direction of both the wire and the contact pad along the positive

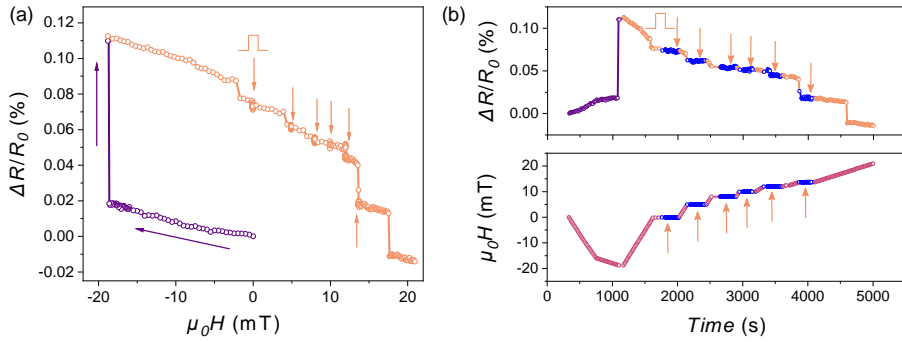


Figure 4.6: Current Induced DW motion. (a) The field is first swept from 0 mT to  $-19.5$  mT to pin the DW (purple curve) and then the field is lowered to 0 mT to attempt depinning of the DW by applying pulses (orange curve) at magnetic fields indicated by the orange arrows. No depinning is observed until the depinning field is reached at  $16.7$  mT. (b) Upper panel: time dependent change in the MR when applying the pulses. The purple curve is prior to pinning, the pulse events are indicated by orange arrows, the data points taken during the pulse events are blue. Lower panel: the changes in applied field as function of time.

x-axis corresponding to low resistance state. We reduced the field to 0 mT and then increased it along the negative x-axis (the negative quadrant) until we saw the sharp increase in  $R$  that is the signature of catching a magnetic domain wall, at  $-19.5$  mT. Next, we reversed the sweep direction until we reached the low resistance state again, corresponding to the depinning field of the DW at  $16.7$  mT. The same experiment was performed in the positive quadrant (see Fig. 4.5(b)). We observed small jumps in resistance before reaching the depinning field, which we attribute to changes in the spin texture of the magnetic domain wall in the notch. The variations are approximately the same in both experiments, as required by the symmetry of magnetic states under positive and negative magnetic fields along the x axis. The slight differences come from the asymmetry in the sample due to the notch and small irregularities along the edges of the wires.

### 4.3.2. Pulse measurements on CrO<sub>2</sub>

Following the field-driven measurements, we applied the pulses. Again, the DW was pinned at the notch, following the procedure outlined above. Next, we changed the field back to 0 mT and injected pulses (frequency : 10 MHz, duty cycle : 20%, single pulse) at the fields indicated in Fig. 4.6 (a). The amplitude was increased in steps of 0.1 V starting from an initial value of 1 V (peak) until reaching a maximum value of 10 V corresponding to an estimated current of 18 mA and a critical current density of  $7.5 \times 10^{11}$  A/m<sup>2</sup>. We did not see any change in the resistance, indicating that the DW was not depinned. Following that, we increased the field along + x-axis in steps

#### 4.4. DW motion in Py nanowires

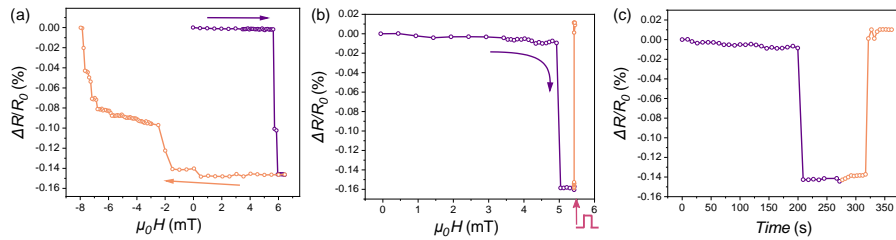


Figure 4.7: Current Induced DW motion in a Py sample. (a) The field is swept from 0 mT to 6 mT where pinning occurs (purple curve). Then the field is swept back to 0 mT and further increased until depinning occurs at -8 mT (orange curve). (b) The field is swept from 0 mT to 5 mT to pin the DW (purple curve). Then it is further increased to 5.5 mT and pulses are applied to depin the DW (orange curve). (c) Time dependent MR to show pinning and depinning events of the plot shown in (b).

(shown with orange arrow in Fig.4.6(a) to value of 5, 7.5, 10, 12.5) mT to 'field-assist' the depinning, since an increased field could help to reduce the critical current density required for depinning, and repeated the pulse injection and resistance measurement. Fig. 4.6 (b) top and bottom shows the moments in time (s) where the pulses were injected with arrows (orange) indicating clearly that the depinning did not occur when pulses were injected. Instead, the changes in resistances and finally depinning happened at the original and unchanged field value of ~ 17 mT.

We conducted the same measurement on additional  $\text{CrO}_2$  devices with similar dimensions but featuring shallower notch width up to 150 nm. However, the results did not change. To understand this better, we next turned to similar measurements on Py devices.

#### 4.4. DW motion in Py nanowires

Py samples have been studied extensively with respect to DW motion [4, 5, 21, 22]. We fabricated a Py-Cu device of the dimensions similar to  $\text{CrO}_2$  device :  $w = 500$  nm,  $t = 50$  nm and  $l = 1.5$   $\mu\text{m}$ . The centre of the wire was milled using FIB to make a double notch where the width of the Py wire is ~ 101 nm. We first performed the field-driven DW motion experiments, as shown in Fig. 4.7a. The field was initially set to -500 mT to saturate the magnetization of the Py device. Then, we swept the field in opposite direction starting from 0 mT until we observed a sharp decrease in the resistance and a low resistance state corresponding to the pinning field of DW at 6 mT. Remember that for Py, the low resistance state means a domain wall is present in the notch. After that, we swept back the field along the negative x-axis until we got back the high resistance state corresponding to the depinning field of the DW at -8 mT.

Next, we conducted the pulse assisted DW depinning measurements. First, we pinned the DW at the notch with the help of the field following the steps as described above and shown in Fig. 4.7(a) and (b) in purple. In the next step (not shown), we reduced the field to 4 mT and injected the pulses (frequency: 10 MHz, duty cycle: 20%, single pulse). However, we did not see the resistance returning to the starting level, even at the maximum applied current, estimated to correspond to  $1.9 \times 10^{11}$  A/m<sup>2</sup>. On the other hand, when we further *increased* the field from 5 mT (the pinning field) to 5.5 mT, we observed the resistance changed from low resistance state to high resistance state at the maximum applied current as shown in Fig. 4.7(b). Fig. 4.7(c) shows the plot of the time dependent change in MR. We see that when we started to apply the pulses of lower current on the device, the resistance stayed at the low level and only at maximum  $J_c$ , the resistance level jumped back to the starting level. This corresponds to the successful depinning of the DW from the notch.

The pulse measurements on Py-Cu demonstrated successful injection of pulses on our devices. However, we also recognized that higher currents were needed for further measurements. The setup's initial configuration imposes a limitation on the current that can be applied, primarily due to the presence of a series resistance of 500  $\Omega$ , which was incorporated into the initial design of the setup as a preventive measure, to safeguard the device against excessive heating caused by high current densities. To address this issue, we made adjustments to the setup by eliminating the series resistance R5 (500  $\Omega$ ), as well as the parallel resistance R4 (53.6  $\Omega$ ). These modifications are shown in Fig. 4.4. In the revised setup, the resistance of the sample is initially measured at 10 K. Based on the resistance value obtained, either a series or parallel resistor of desired value was added. This addition was necessary to achieve a total impedance of approximately 50  $\Omega$ , which is the desired value for optimal transmission. This enabled us to increase the current density by one order of magnitude.

## 4.5. DW motion in Py nanowires in the modified setup

After the modifications in the setup, we tested it with the Py-Cu devices. For this, we made similar Py nanowire device as shown in Fig. 4.3(a) of the following dimensions:  $w = 500$  nm,  $t = 50$  nm and  $l = 1.5$   $\mu$ m. The centre of the wire has a double notch where the width of the Py wire is 175 nm. After the standard characterization processes where we measured the resistivity and the MR hysteresis loop, we attempted the pulse measurements. First, we pinned the DW at the notch with the help of the field and then attempted to depin the DW by gradually increasing the current of

---

All DW measurements were studied at 10 K in the modified setup

#### 4.5. DW motion in Py nanowires in the modified setup

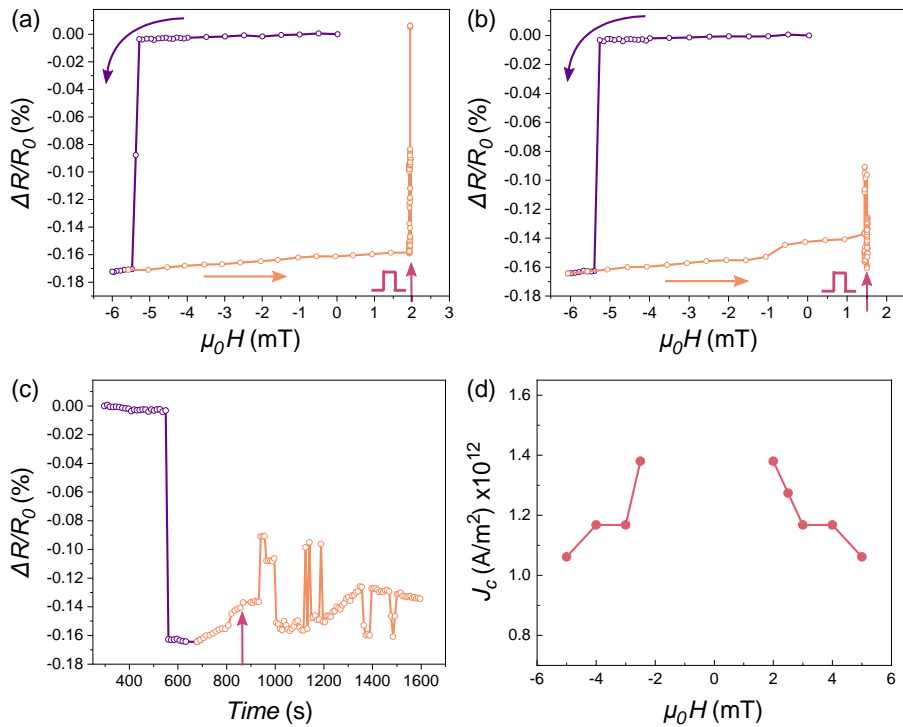


Figure 4.8: Pulse measurement on a Py sample in the modified setup. (a) Field is swept from 0 mT to  $-5.5$  mT where pinning occurs (purple curve) and then field is reversed and swept back till 2 mT (orange curve) and pulse is applied (red arrow) to depin (orange curve). (b) Same as in (a) but now the pulse is applied at field of 1.5 mT. (c) Time dependent MR to show pinning and pulse events for the plot shown in (b). Arrow indicates point in time 1.5 mT was reached. (d) Critical current density as a function of field needed to depin shows that as the field is decreased towards 0 mT from either side the depinning current density increases.

the injected pulses. In Fig. 4.8(a) we show the successful depinning at 2 mT which was the lowest field where we could successfully depin the DW. Fig. 4.8(b,c) show the unsuccessful pulse-assisted depinning attempt at 1.5 mT. We measured the depinning current density at different fields as shown in Fig. 4.8(d), starting from  $\pm 5$  mT and decreasing the field in steps of 1 mT. At  $\pm 5$  mT, we found that  $J_c$  was  $1.06 \times 10^{12}$  A/m<sup>2</sup> which increased to  $1.38 \times 10^{12}$  A/m<sup>2</sup> at  $\pm 2$  mT. As expected,  $J_c$  started to increase as we approached 0 mT field from either direction.

We next made changes to the dimensions of the sample to further reduce the field needed to depin. We fabricated a Py device as shown in Fig. 4.9(a) with  $w = 253$  nm,  $t = 40$  nm and  $l = 1.5$   $\mu$ m. The centre of the wire has a single notch where the width of the Py wire is 150 nm. We performed the standard characterization

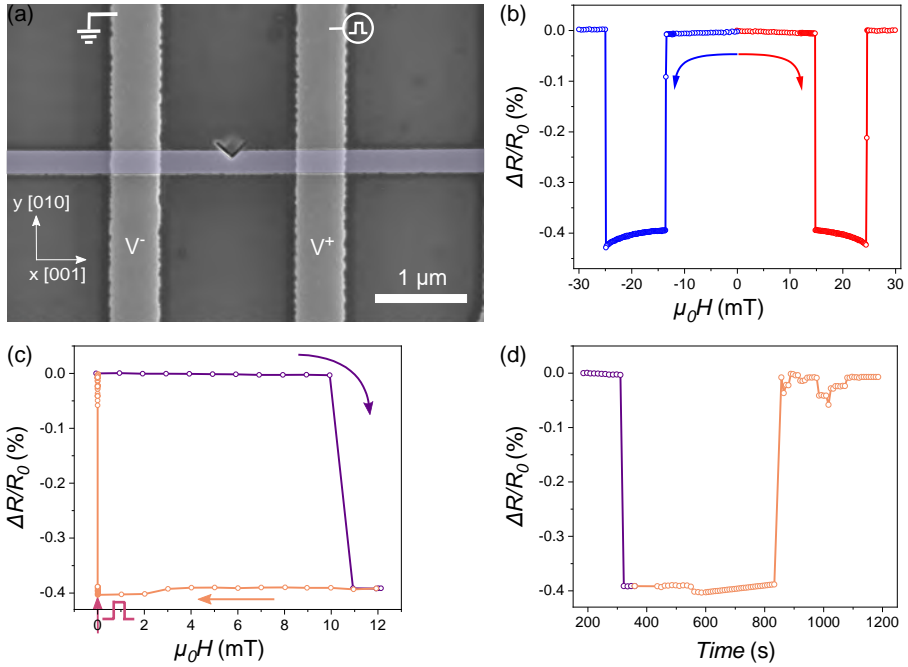


Figure 4.9: Pulse measurement on Py sample in modified setup. (a) SEM image of the Py device (the Py wire shown in false color is along [001]). The center of the wire has a single notch made with Focused Ion Beam milling. (b) In-plane longitudinal magnetoresistance along [001], measured at 10 K by sweeping the magnetic field from 0 mT to 30 mT (red curve) and 0 mT to -30 mT (blue curve). The step size is 0.5 mT. The current used for the MR measurement is 100  $\mu\text{A}$ . (c) A pulse measurement. The field is swept from 0 mT to 12 mT where pinning occurs (purple curve). Then the direction is reversed and swept back to 0 mT. At that field, a pulse is applied (red arrow) to depin (orange curve). The critical depinning current density ( $J_c$ ) is calculated to be  $2.85 \times 10^{12} \text{ A/m}^2$ . (d) Time dependent MR to show pinning and depinning events for the plot shown in (c).

processes where we measured the resistivity and the MR hysteresis loop before attempting the pulse measurements. The decreased width and thickness of the wire results in higher pinning and depinning fields as seen in Fig. 4.9(b). We also observed that the change in resistance ( $\Delta r_{DW}$ ) between single domain state and DW state has more than doubled.

Next, we attempted the pulse measurement on the sample by field assisted pinning of DW and then followed by pulse assisted depinning. As seen in Fig. 4.9(c), we were able to successfully depin at zero field by applying pulses corresponding to a current density  $J_c$  of  $2.85 \times 10^{12} \text{ A/m}^2$ . This pulse assisted depinning at zero field for Py sample shows that setup is working and that we fixed the initial issues of too low current injection. After this, we moved back to CrO<sub>2</sub> devices to attempt the pulse measurements.

## 4.6. DW motion in CrO<sub>2</sub> nanowires in the modified setup

We fabricated a CrO<sub>2</sub> sample as shown in Fig. 4.10(a) with  $w = 625$  nm,  $t = 80$  nm and  $l = 4$   $\mu$ m. The centre of the wire has a double notch where the width of the CrO<sub>2</sub> wire is 475 nm. After initial resistivity measurements, we first performed a field driven DW motion without pulses to measure the depinning field of  $-5.3$  mT, shown in Fig.4.10(b), and  $5.1$  mT, shown in Fig. 4.10(c). We also notice that the percentage change in MR has lowered from nearly 0.15 % as seen in Fig. 4.1 (c) for a neck width of 91 nm to approximately 0.02 % when the neck width is 475 nm. The depinning field has also decreased, from nearly  $\pm 17$  mT as seen in Fig. 4.5 (a) and (b) to nearly  $\pm 5$  mT.

Next, we attempted the pulse assisted depinning measurements on the sample. We observed successful depinning through pulse injection as shown in Fig. 4.10 (d,e) for fields above and including  $\pm 3$  mT. However, we could not depin below 3 mT. Fig. 4.10(g) gives the plot of the depinning current density ( $J_c$ ) as a function of the field. At  $\pm 6$  mT, the value for  $J_c$  was  $1.5 \times 10^{11}$  A/m<sup>2</sup>, which increased by a factor 6 to  $9.7 \times 10^{11}$  A/m<sup>2</sup> when field was reduced to 3 mT. We observed a small asymmetry in  $J_c$ , which may be attributed to the intrinsic asymmetry of the device. Furthermore, it is evident, as expected, that the size of the notch makes an impact to  $J_c$ . While a deep notch assists in obtaining a strong MR signal, it also leads to strong pinning potential for both Py and CrO<sub>2</sub> samples which makes depinning challenging. Conversely, a shallow notch makes the DW's pinning weaker, but it facilitates depinning during pulse measurements.

Finally, similar to the Py samples, we attempted to make a single notch on the CrO<sub>2</sub> wire as shown in Fig. 4.11(a) of similar width of 625 nm and thickness of 91 nm. The wire width at the notch is around 450 nm. The MR hysteresis loop displayed in Fig. 4.11(b) shows similar behavior as the previous sample with double notch (see Fig. 4.10(b,c)) with a MR change of around 0.025%. For this sample, we could depin using pulses until 5 mT.  $J_c$  was calculated to be  $6.8 \times 10^{11}$  A/m<sup>2</sup> which is about 2.5 times higher than  $2.5 \times 10^{11}$  A/m<sup>2</sup> measured for the previous sample. This indicates, not surprisingly, that the CrO<sub>2</sub> devices are very sensitive to variations in the width of the notch and probably also the shape of the notch. The depinning current density reveals a sharp rise even in response to minor variations in the devices. As seen in Fig. 4.11(c), we could not depin at field of 4 mT and below while in the last device it was possible to depin up to 3 mT.

Another significant point is that we used evaporation and liftoff methods to deposit Py-Cu samples in order to fabricate the devices. This provided us with the ability to control the thickness of the nanowires. However, in the case of CrO<sub>2</sub>, we used Chemical Vapor Deposition technique to grow CrO<sub>2</sub>. This makes achieving

#### 4. Moving Domain Walls in Permalloy and CrO<sub>2</sub> Nanowires

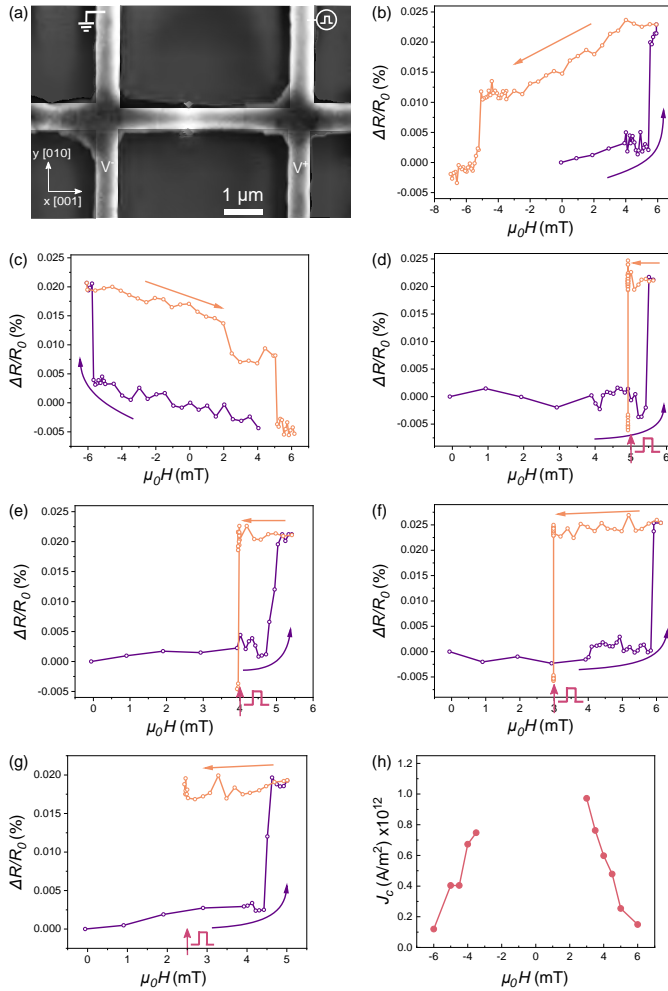


Figure 4.10: Pulse measurement on a CrO<sub>2</sub> sample in the modified setup. (a) SEM image of the CrO<sub>2</sub> device (see details in the text). The length of the wire is along [001]. The center of the wire has a small double notch made with FIB milling. (b) The field is swept from 0 mT to 5 mT where we see the change in resistance (from low to high resistance) corresponding to DW pinning (purple curve). Then the field is swept back until we obtain the low resistance state (orange curve) corresponding to the depinning field at -5.3 mT. (c) Same as in (b) but in the reversed direction. We find the pinning field at -5.5 mT and the depinning field at 5.1 mT. (d), (e), (f), (g) The field is swept from 0 mT to 5.3 mT where pinning occurs (purple curve) and then swept back until 5 mT, 4 mT, 3 mT and 2.5 mT (orange curve) respectively. At these fields, pulses are applied (red arrow) to depin (orange curve). (h) Critical current density as a function of field needed to depin. As the field is decreased towards 0 mT from either side the depinning current density increases. There was no depinning found between -2.5 mT and 2.5 mT.

#### 4.6. DW motion in CrO<sub>2</sub> nanowires in the modified setup

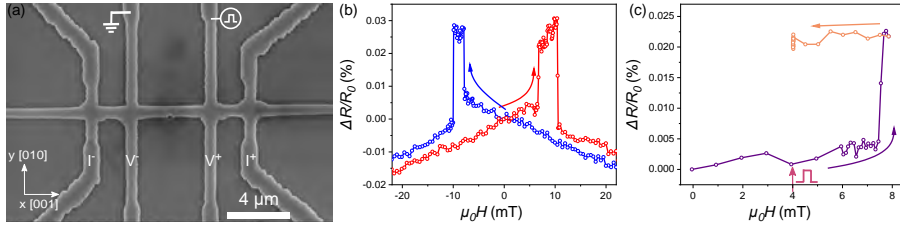


Figure 4.11: Pulse measurement on a CrO<sub>2</sub> sample in the modified setup. (a) SEM image of the CrO<sub>2</sub> device (see details in the text). The length of the wire is along [001]. The center of the wire has a small single notch made with FIB milling. (b) In-plane longitudinal magnetoresistance along [001], measured at 10 K by sweeping the magnetic field between +30 mT and -30 mT. The current used in the MR measurement is 100  $\mu$ A. (c) The field is swept from 0 mT to 7.5 mT where pinning occurs (purple curve). Then field is reversed and swept back until 4 mT (orange curve) and a pulse is applied (red arrow) to attempt depinning (orange curve).

precise control over the thickness of the nanowires more challenging. Hence, it was not easy to grow thin nanowires in the range of 10 – 40 nm which has been used in previous studies on other ferromagnets [4, 5, 22]. In order to address this issue, attempts were made to remove the top layer of CrO<sub>2</sub> devices using an Argon (Ar) etcher. However, that resulted in no pinning of DW (see Appendix Fig. 4.13). This lack of pinning may likely be attributed to the surface being damaged during the etching process and the introduction of contaminants from the use of Ar ions. Another experimental approach that we would have been interested in pursuing, but were unable to, owing to challenges in growth and fabrication process, included reducing the width of the CrO<sub>2</sub> wire. This was motivated by our findings indicating that decreasing wire width had a positive effect on depinning in the instance of Py.

An important factor that merits consideration is Joule heating. The injection of pulses results in high currents and current densities due to small dimensions of our devices, and heating is a well-known issue in the study of current-induced domain wall motion, mostly performed on Py. When similar measurements are performed at room temperature, the observed effect becomes more significant since the temperature may approach the Curie temperature ( $T_C$ ). In certain cases, when these measurements are conducted at room temperature the effect may even exceed  $T_C$  [7, 22]. However, when the measurements were conducted at low temperatures, the effect is diminished. Laufenberg et. al. [22], working with Py rings, showed that below 20 K the sample heats up by  $\Delta T \approx 100$  K at a current density of  $2.1 \times 10^{12}$  A/m<sup>2</sup> when applying pulses. Biehler et al. observed similar results below 50 K on CrO<sub>2</sub> wires etched out of films [8]. In our case, we conducted all the pulse measurements at 10 K. This most likely suggests that while the actual sample temperature of the sample may well be significantly higher than 10 K, it will still remain significantly lower than the  $T_C$  of about 650 K for Py and 390 K for CrO<sub>2</sub>.

## 4.7. Conclusion

In summary, we have built and developed a high frequency setup to study current driven domain wall motion. The setup allows to inject current pulses to assist in depinning of DW. The setup was tested on Py samples and the critical fields and critical current densities necessary to move a domain wall in Py nanowires were measured. The pulse measurements on different widths and thickness of Py nanowires show that, the depinning is easier on a narrow and shallow notched wire (< 30%) as compared to wider wires and deep notch.

In CrO<sub>2</sub> nanowires, the temperature dependence of MR effects was studied. We observed that  $\Delta r_D$  initially decreased between 10 and 80 K and above 80 K, started to increase, although the trend was not clear above 150 K due to difficulty in measuring a clear and sharp MR signal. CrO<sub>2</sub> samples also show that it is possible to move a DW using pulses. However, depinning current density increases sharply with decreasing magnetic field as compared to Py devices where the rise in current density is gradual. Furthermore, CrO<sub>2</sub> devices are more sensitive to the width of the notch and slight variations can bring about a large change in depinning current density. The magnitude of critical current densities are comparable to that of Py samples and high spin polarization does not reduce the current densities. The main difficulty with CrO<sub>2</sub> remains it's extremely difficult and sensitive fabrication process which makes it hard to systematically study to make fast progress with the measurements.

## 4.8. Appendix

### 4.8.1. Pulse measurement on a Py-Cu device with a deep notch in the modified setup

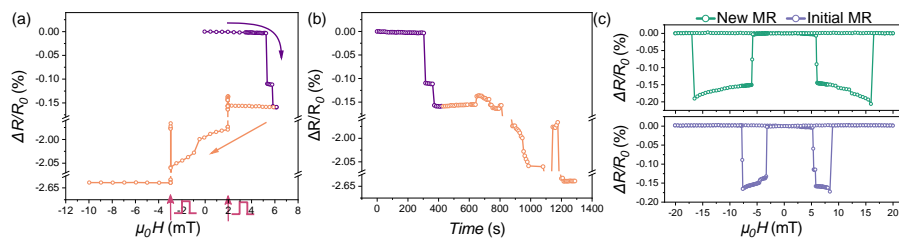


Figure 4.12: Pulse measurement on a Py-Cu device in the modified high frequency setup. (a) The field is swept from 0 mT to 5.5 mT where pinning occurs (purple curve). Then the field is swept back until 2 mT (orange curve) and pulses are applied (red arrow) to attempt depinning. The resistance decreases sharply on applying the pulse, indicating damage to the device. Afterwards, the field was further swept to  $-3$  mT and pulses were again injected. The resistance dropped again. (b) The time dependent MR plot of (a) shows the drop in resistance when pulses are applied. (c) Comparison between the MR plots before injecting any pulses to the device (blue curve) and after injecting pulses (green curve) in the same device. The depinning of the DW with pulses does not work anymore at any field including 5 mT.

A Py-Cu device of the following dimensions:  $w = 500$  nm,  $t = 50$  nm,  $l = 1.5$   $\mu\text{m}$  and notch width = 165 nm was measured in the modified high frequency setup. The pulse assisted depinning worked normally above 2 mT. However, at 2 mT and below, the depinning did not work. When the pulses were injected, we observed a sharp drop in resistance instead of the resistance going up as usual. The corresponding current density was  $5.4 \times 10^{12}$  A/m<sup>2</sup>. This change of resistance was permanent and probably came from damage to the device due to the high current. After several failed attempts with the pulse measurement at different fields, where we observed similar sharp drop in resistance, we measured the MR hysteresis loop of the sample again. As seen in Fig. 4.12(c), we find that the behavior has changed from the last measurement. The low resistance state window in new MR has become very wide compared to the initial MR. Also, now the depinning of DW with pulses does not work anymore at any field including 5 mT, suggesting damage to the sample from the high current. To better understand the damage caused to the device, we would need further investigation.

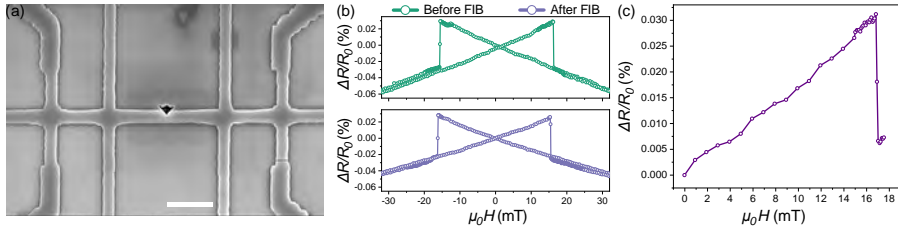
4.8.2. Measurements on an Ar etched CrO<sub>2</sub> device with a single notch

Figure 4.13: (a) SEM image of a CrO<sub>2</sub> device width  $w = 431$  nm,  $t = 82$  nm,  $l = 4$   $\mu\text{m}$  and notch width = 355 nm after FIB. (b) Comparison between the MR plots following a 2-minute argon (Ar) etching process on a CrO<sub>2</sub> device both before FIB (green curve) and after making a notch with FIB (blue curve) shows almost no change in MR plot. (c) Failed attempt to pin the DW using field. Instead we see an instantaneous change in magnetization direction from negative x-axis to positive x-axis.

In the preceding sections, we observed in Py-Cu devices that a decrease in the thickness of the Py wire allowed for the depinning of DW to occur at lower fields with the pulse injection. We attempted to replicate the same with CrO<sub>2</sub> wire. Due to the challenges encountered in achieving the desired thin wire growth using CVD compared to the evaporation for Py wires, we Ar-etched the CVD grown wire of dimensions width  $w = 431$  nm,  $t = 82$  nm and  $l = 4$   $\mu\text{m}$ , for 2-min to thin it down. Following the Ar-etch,  $t$  was measured to be around 75 nm. Fig. 4.13(b) shows the MR plot (green curve) of the wire after Ar-etching. Since, the MR doesn't show pinning of a DW, we made a notch using FIB similar to other devices. Fig. 4.13(a) gives the SEM image of the wire with a single notch after FIB milling. Next, we measured the MR again and found the plot (blue curve) to be of same nature as for the wire before FIB. This observation suggests that notch didn't help with pinning the DW, which typically appears as a high resistance state within a narrow range of applied magnetic field before transitioning to a low resistance state, as we had found for earlier devices which were not etched. One of the plausible reason could be that Ar-etching leads to damage to the surface of CrO<sub>2</sub> wire which affects the pinning site. Fig. 4.13(c) gives one of the failed attempts to pin the DW on this wire. Instead of a high resistance state, we observed an instantaneous change in magnetization direction from - x-axis to + x-axis.

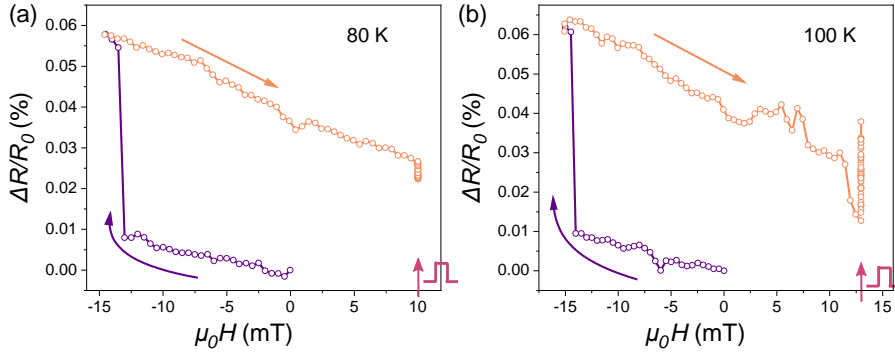
4.8.3. Pulse measurement on a  $\text{CrO}_2$  device at 80 K and 100 K

Figure 4.14: Pulse measurement on  $\text{CrO}_2$  device at 80 K and 100 K. (a) Pulse measurement at 80 K. Field is swept from 0 mT to  $-14.5$  mT where pinning occurs (purple curve) and then field is reversed and swept back till 10 mT (orange curve) and pulse is applied (red arrow) to attempt depin (orange curve). (b) Pulse measurement at 100 K. Field is swept from 0 mT to  $-15$  mT where pinning occurs (purple curve) and then field is reversed and swept back till 13 mT (orange curve) and pulse is applied (red arrow) to attempt depin (orange curve). In both cases, the depinning didn't occur.

As discussed before in sec.4.3, pulse measurements were attempted on a  $\text{CrO}_2$  device (see Fig. 4.1 (a) of  $w = 500$  nm,  $t = 60$  nm and  $l = 1.5$   $\mu\text{m}$ , with a central double notch of width around 91 nm) at 10 K in the initial high frequency set up. After, the failed attempts of depinning DW at 10 K, we also attempted the pulse measurements at higher temperatures of 80 K and 100 K. As shown in Fig. 4.14 (a) and (b), depinning was not observed for either temperature.

---

## References

- [1] Allwood, D. A. et al. Magnetic domain-wall logic. Science **309**, 1688–1692 (2005).
- [2] Parkin, S. S. P., Hayashi, M. & Thomas, L. Magnetic domain-wall racetrack memory. Science **320**, 190–194 (2008). URL <https://www.science.org/doi/abs/10.1126/science.1145799>. <https://www.science.org/doi/pdf/10.1126/science.1145799>.
- [3] Berger, L. Emission of spin waves by a magnetic multilayer traversed by a current. Phys. Rev. B **54**, 9353–9358 (1996). URL <https://link.aps.org/doi/10.1103/PhysRevB.54.9353>.
- [4] Yamaguchi, A. et al. Real-space observation of Current-Driven Domain Wall Motion in Submicron Magnetic Wires. Phys. Rev. Lett. **92**, 077205 (2004). URL <https://link.aps.org/doi/10.1103/PhysRevLett.92.077205>.
- [5] Kläui, M. et al. Controlled and reproducible domain wall displacement by current pulses injected into ferromagnetic ring structures. Phys. Rev. Lett. **94**, 106601 (2005). URL <https://link.aps.org/doi/10.1103/PhysRevLett.94.106601>.
- [6] Hayashi, M. et al. Dependence of current and field driven depinning of domain walls on their structure and chirality in permalloy nanowires. Phys. Rev. Lett. **97**, 207205 (2006). URL <https://link.aps.org/doi/10.1103/PhysRevLett.97.207205>.
- [7] Yamaguchi, A. et al. Effect of joule heating in current-driven domain wall motion. Appl. Phys. Lett. **86**, 046602 (2004). URL <https://aip.scitation.org/doi/10.1063/1.1847714>.
- [8] Biehler, A. et al. Domain structures and the influence of current on domains and domain walls in highly spin-polarized  $\text{CrO}_2$  wire elements. Phys. Rev. B **75**, 184427 (2007). URL <https://link.aps.org/doi/10.1103/PhysRevB.75.184427>.
- [9] Laufenberg, M. Interactions Between Current and Domain Wall Spin Structures. Ph.D. thesis, Universität Konstanz, Germany (2006).
- [10] König, C. Nanomagnetismus von epitaktischen Fe (110)- und  $\text{CrO}_2$  (100)-Strukturen im Hinblick auf potentielle spinelektronische Anwendungen. Ph.D. thesis, Aachen, Techn. Hochsch., Diss., 2006, Germany (2006).

- [11] Chen, W., Qian, L. & Xiao, G. Resistance of domain-wall states in half-metallic  $\text{CrO}_2$ . *Phys. Rev. B* **98**, 174402 (2018). URL <https://doi.org/10.1103/PhysRevB.98.174402>.
- [12] Chiba, D. *et al.* Control of multiple magnetic domain walls by current in a co/nl nano-wire. *Applied Physics Express* **3**, 073004 (2010). URL <https://dx.doi.org/10.1143/APEX.3.073004>.
- [13] Koyama, T. *et al.* Observation of the intrinsic pinning of a magnetic domain wall in a ferromagnetic nanowire. *Nature Materials* **10**, 194–197 (2011). URL <https://doi.org/10.1038/nmat2961>.
- [14] Yao, J. *Spin Transport and Superconductivity in Half-metallic Nanowires and Junctions*. Ph.D. thesis, Leiden University (2023).
- [15] Kent, A. D., Yu, J., Rüdiger, U. & Parkin, S. S. Domain wall resistivity in epitaxial thin film microstructures. *Journal of Physics: Condensed Matter* **13**, R461 (2001).
- [16] Zou, X. *Magnetic Domain Configurations and Huge Wall Resistivity in Half-metallic Chromium Dioxide ( $\text{CrO}_2$ ) Nanostructures*. Ph.D. thesis, Brown University, Providence, Rhode Island, 5 (2010).
- [17] Levi, P. & Zhang, S. Resistivity due to domain wall scattering. *Phys. Rev. Lett.* **79**, 5110 (1997). URL <https://doi.org/10.1103/PhysRevLett.79.5110>.
- [18] Viret, M. *et al.* Spin scattering in ferromagnetic thin films. *Phys. Rev. B* **53**, 8464 (1996). URL <https://doi.org/10.1103/PhysRevB.53.8464>.
- [19] Ye, J. *et al.* Berry phase theory of the anomalous hall effect: Application to colossal magnetoresistance manganites. *Phys. Rev. Lett.* **83**, 3737 (1999). URL <https://doi.org/10.1103/PhysRevLett.83.3737>.
- [20] Yanagihara, H. & Salamon, M. B. Skyrmion strings and the anomalous hall effect in  $\text{CrO}_2$ . *Phys. Rev. Lett.* **89**, 187201 (2002). URL <https://doi.org/10.1103/PhysRevLett.89.187201>.
- [21] Vernier, N., Allwood, D. A., Atkinson, D., Cooke, M. D. & Cowburn, R. P. Domain wall propagation in magnetic nanowires by spin-polarized current injection. *Europhysics Letters* **65**, 526 (2004). URL <https://dx.doi.org/10.1209/epl/i2003-10112-5>.
- [22] Laufenberg, M. *et al.* Temperature dependence of the spin torque effect in current-induced domain wall motion. *Phys. Rev. Lett.* **97**, 046602 (2006). URL <https://link.aps.org/doi/10.1103/PhysRevLett.97.046602>.